



Evaluation of 3D Printed Gelatin-Based Scaffolds with Varying Pore Size for MSC-Based Adipose Tissue Engineering

Liesbeth Tytgat, Matthias R. Kollert, Lana Van Damme, Hugo Thienpont, Heidi Ottevaere, Georg N. Duda, Sven Geissler, Peter Dubruel, Sandra Van Vlierberghe,* and Taimoor H. Qazi*

Adipose tissue engineering aims to provide solutions to patients who require tissue reconstruction following mastectomies or other soft tissue trauma. Mesenchymal stromal cells (MSCs) robustly differentiate into the adipogenic lineage and are attractive candidates for adipose tissue engineering. This work investigates whether pore size modulates adipogenic differentiation of MSCs toward identifying optimal scaffold pore size and whether pore size modulates spatial infiltration of adipogenically differentiated cells. To assess this, extrusion-based 3D printing is used to fabricate photo-crosslinkable gelatin-based scaffolds with pore sizes in the range of 200–600 μm . The adipogenic differentiation of MSCs seeded onto these scaffolds is evaluated and robust lipid droplet formation is observed across all scaffold groups as early as after day 6 of culture. Expression of adipogenic genes on scaffolds increases significantly over time, compared to TCP controls. Furthermore, it is found that the spatial distribution of cells is dependent on the scaffold pore size, with larger pores leading to a more uniform spatial distribution of adipogenically differentiated cells. Overall, these data provide first insights into the role of scaffold pore size on MSC-based adipogenic differentiation and contribute toward the rational design of biomaterials for adipose tissue engineering in 3D volumetric spaces.

of malignant tumors.^[2,3] Current reconstruction strategies including implants, lipofilling, and microsurgical free tissue transplantation are associated with disadvantages such as capsular contracture, high resorption rates, and microsurgical complications.^[4] Therefore, new bioengineering strategies to repair soft tissue defects have gained increasing scientific and medical interest.

Adipose tissue engineering is a promising strategy to repair soft tissue defects by combining mesenchymal stromal cells (MSCs) with biomaterials to create stable, bioactive constructs that enable 3D adipose tissue regeneration.^[4] Gelatin is a frequently applied biomaterial due to its cell-interactive properties and close resemblance to collagen, which is the main component of the extracellular matrix of adipose tissue.^[5–7] Photo-crosslinkable methacrylated gelatin (Gel-MA) is a widely used hydrogel and has previously been used to culture adipose derived cells in 3D

Breast cancer is the most common type of cancer occurring in women worldwide^[1] and accordingly, there is an exponential growth of reconstruction procedures performed in the clinic to repair soft tissue defects resulting from the resection


confining environments to study the role of stiffness on lipid droplet formation.^[8,9] In the present work, we explored the adipogenic differentiation behavior of bone-marrow-derived MSCs in porous 3D scaffolds that do not confine cells but rather allow

L. Tytgat, L. Van Damme, Prof. P. Dubruel, Prof. S. Van Vlierberghe
Polymer Chemistry & Biomaterials Group
Centre of Macromolecular Chemistry (CMaC)
Ghent University
Krijgslaan 281, S4-Bis, 9000 Ghent, Belgium
E-mail: Sandra.vanvlierberghe@ugent.be

L. Tytgat, Prof. H. Thienpont, Prof. H. Ottevaere, Prof. S. Van Vlierberghe
Brussels Photonics
Vrije Universiteit Brussel
Pleinlaan 2, 1050 Brussels, Belgium

M. R. Kollert, Dr. G. N. Duda, Prof. S. Geissler, Dr. T. H. Qazi
Julius Wolff Institute for Biomechanics and Musculoskeletal Regeneration
Charité Universitätsmedizin Berlin
Augustenburger Platz 1, 13353 Berlin, Germany
E-mail: thqazi@seas.upenn.edu

M. R. Kollert, Dr. G. N. Duda, Prof. S. Geissler, Dr. T. H. Qazi
Berlin-Brandenburg Center and School for Regenerative Therapies
Charité Universitätsmedizin Berlin
Augustenburger Platz 1, 13353 Berlin, Germany
Dr. T. H. Qazi
Department of Bioengineering
University of Pennsylvania
210 South 33rd Street, Philadelphia 19104, USA

 The ORCID identification number(s) for the author(s) of this article can be found under <https://doi.org/10.1002/mabi.201900364>.

© 2020 The Authors. Published by WILEY-VCH Verlag GmbH & Co. KGaA, Weinheim. This is an open access article under the terms of the Creative Commons Attribution-NonCommercial License, which permits use, distribution and reproduction in any medium, provided the original work is properly cited and is not used for commercial purposes.

DOI: 10.1002/mabi.201900364

spatial spreading, movement, and distribution. To do this, we employed additive manufacturing (AM), which affords the possibility of precisely controlling construct parameters including pore size and allows easy modification of design parameters (e.g., scaffold dimensions) via computer-aided design (CAD) software. Furthermore, AM allows the production of patient-specific 3D scaffolds which are based on a predefined CAD model obtained via medical scans of the defect.^[10] Extrusion-based 3D printing is one of the most widespread AM techniques due to its relatively low cost and its wide materials processing range.^[11,12] We envisioned that these types of scaffolds could be used for endogenous adipose tissue engineering. Herein, the 3D scaffolds are produced by pneumatically extruding the material in a layer-by-layer fashion. Subsequently, MSCs were seeded onto the scaffolds to evaluate the effect of scaffold architecture (pore size) on the adipogenic differentiation potential of the MSCs. To the best of our knowledge, this is the first study that uses extrusion-based 3D printed Gel-MA scaffolds to investigate the effect of pore size on the adipogenic differentiation and spatial distribution of MSCs.

Microporous Gel-MA scaffolds with different pore sizes were produced via extrusion-based 3D printing. The different scaffold types were obtained by varying strut spacing from 400 to 800 μm resulting in corresponding pore sizes of $230 \pm 24 \mu\text{m}$ (400), $302 \pm 30 \mu\text{m}$ (500), $348 \pm 28 \mu\text{m}$ (600), and $531 \pm 33 \mu\text{m}$ (800) (Figure 1a,b). Furthermore, scaffolds with a high shape fidelity were obtained by carefully controlling the printing and crosslinking parameters including a constant pressure (120 kPa), temperature (30 $^{\circ}\text{C}$), and writing speed (10 mm s^{-1}).

In addition, a consistent UV exposure time was applied and a high precision nozzle with a diameter of 150 μm was used to ensure the production of stable scaffolds with similar strut widths. Furthermore, the results from the swelling assay indicated that all scaffold types were able to absorb large amounts of water (Figure 1e). However, the scaffolds with larger pore sizes were able to swell more compared to the smaller pore sized scaffolds. The opposite trend was observed for the compressive moduli (Figure 1c,d). These results indicate that there is a correlation between the swelling and mechanical properties of the scaffolds. This is reflected by an increasing mass swelling ratio (40–67) and a decreasing compressive modulus (892–124 Pa) upon increasing pore size. These observations are in agreement with the results obtained earlier by Liu et al. and Li et al., who attributed these results to the lower structural integrity of the scaffolds.^[13,14] Although the stiffness of the extruded Gel-MA across all groups is 3–4 kPa mimicking native soft tissue compliance,^[15] the change in compressive moduli as pore size increases reflects the macroscale structural integrity of the scaffolds. In future work, maintaining low stiffness to promote adipogenic differentiation while improving the structural stability to improve implantation handleability could involve reinforcing the ink with secondary particles or phases.^[16,17]

The ability of Gel-MA scaffolds to support adipogenic differentiation of MSCs was investigated by optical microscopy, fluorescent staining, and gene expression analysis. The expression of characteristic adipogenic markers PPAR- γ , LPL, FABP, and FASN was evaluated in the four scaffold

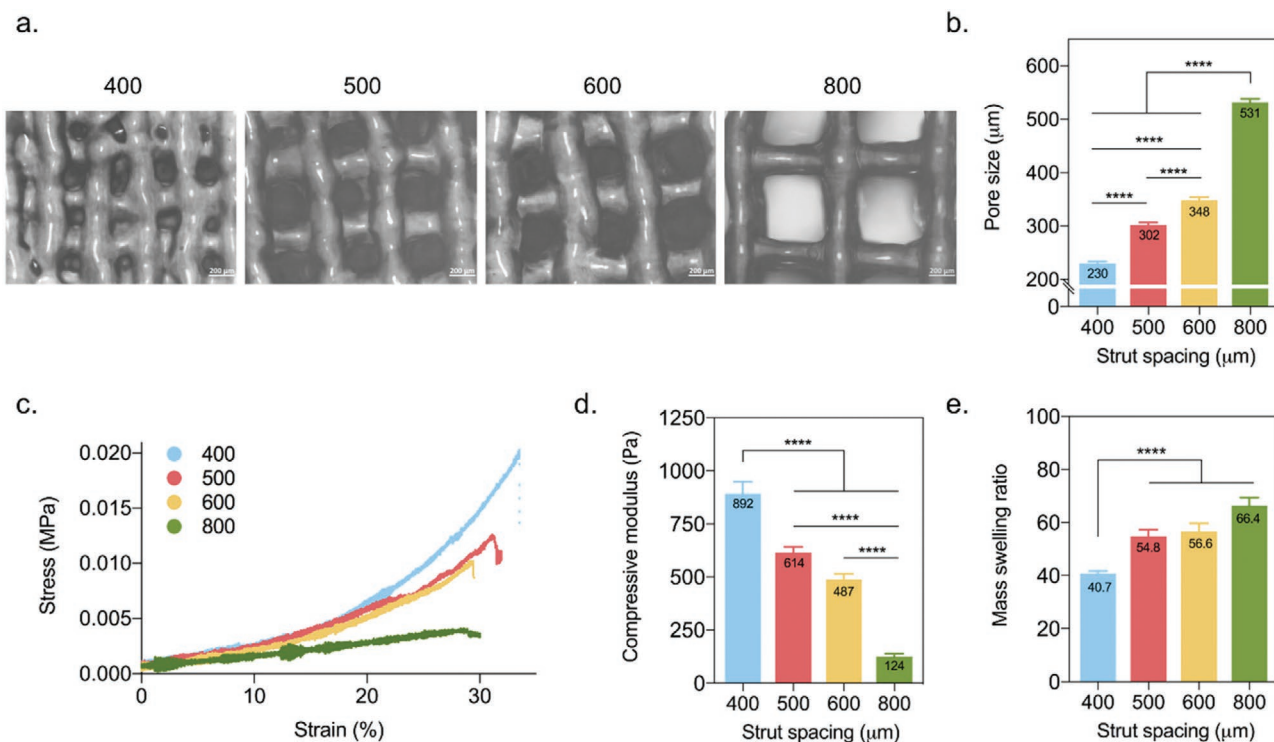


Figure 1. Physico-chemical characterization of the 3D printed Gel-MA scaffolds. a,b) Representative images of the pores together with the pore sizes obtained for the different scaffolds. The scale bars represent 200 μm . c,d) Stress versus strain curves obtained via compression tests from which the compressive modulus is determined. e) Mass swelling ratio of the scaffolds.

groups and in tissue culture plastic (TCP). By day 6 of adipogenic induction, all the characteristic adipogenic markers were expressed significantly higher in all groups (scaffolds as well as TCP) compared to the corresponding controls cultured in expansion media. Lipid droplet formation was observed in all scaffold and TCP groups as early as day 6 of adipogenic stimulation (data not shown), despite the differences in upstream gene expression between TCP and scaffolds. Between day 6 and day 8, MSCs in all scaffold groups showed a significant increase in the expression of adipogenic markers, whereas this was not observed in TCP (Figure 2a). Adipogenically differentiated cells, as identified by the prominent presence of lipid droplets, were observed after 8 days of culture (Figure 2b). For a clear identification and assessment of lipid droplet formation, the cells were stained with Nile Red, a fluorescent dye that specifically binds to lipid droplets, and DAPI to identify nuclei (Figure 2c). Fluorescence images acquired for independent scaffolds with z-stacks up to depths of 100–150 μm showed adipogenically differentiated MSCs distributed on or near the surface of the scaffolds. Absence of lipid droplets in negative control cultures (expansion media

without adipogenic supplements) confirmed the validity of the differentiation protocol. Furthermore, quantification of Nile Red positive area normalized to the cell number revealed significant differences between smaller pore size scaffolds (strut spacing of: 400 and 500) and the larger pore size scaffolds (strut spacing of: 600 and 800), with a higher normalized Nile Red positive area observed for larger pore size scaffolds (Figure 2d). One of the characteristics of mature adipogenic phenotype is a higher lipid content within cells; although we did not perform advanced single cell microscopy to determine this, the quantitative data in Figure 2d points to this direction with scaffolds showing the highest and TCP showing the lowest Nile red positive area per nuclei.^[18] Paradoxically, cells stimulated on TCP substrates showed the highest gene expression compared to scaffolds at both time points; this may be due to differences in expression of genes and mRNA translation. This may indicate that soft scaffolds that faithfully mimic some of the environmental conditions promote a mature phenotype of differentiated cells over time compared to TCP. These findings further indicate that in addition to adipose derived MSCs (ASCs), which owing

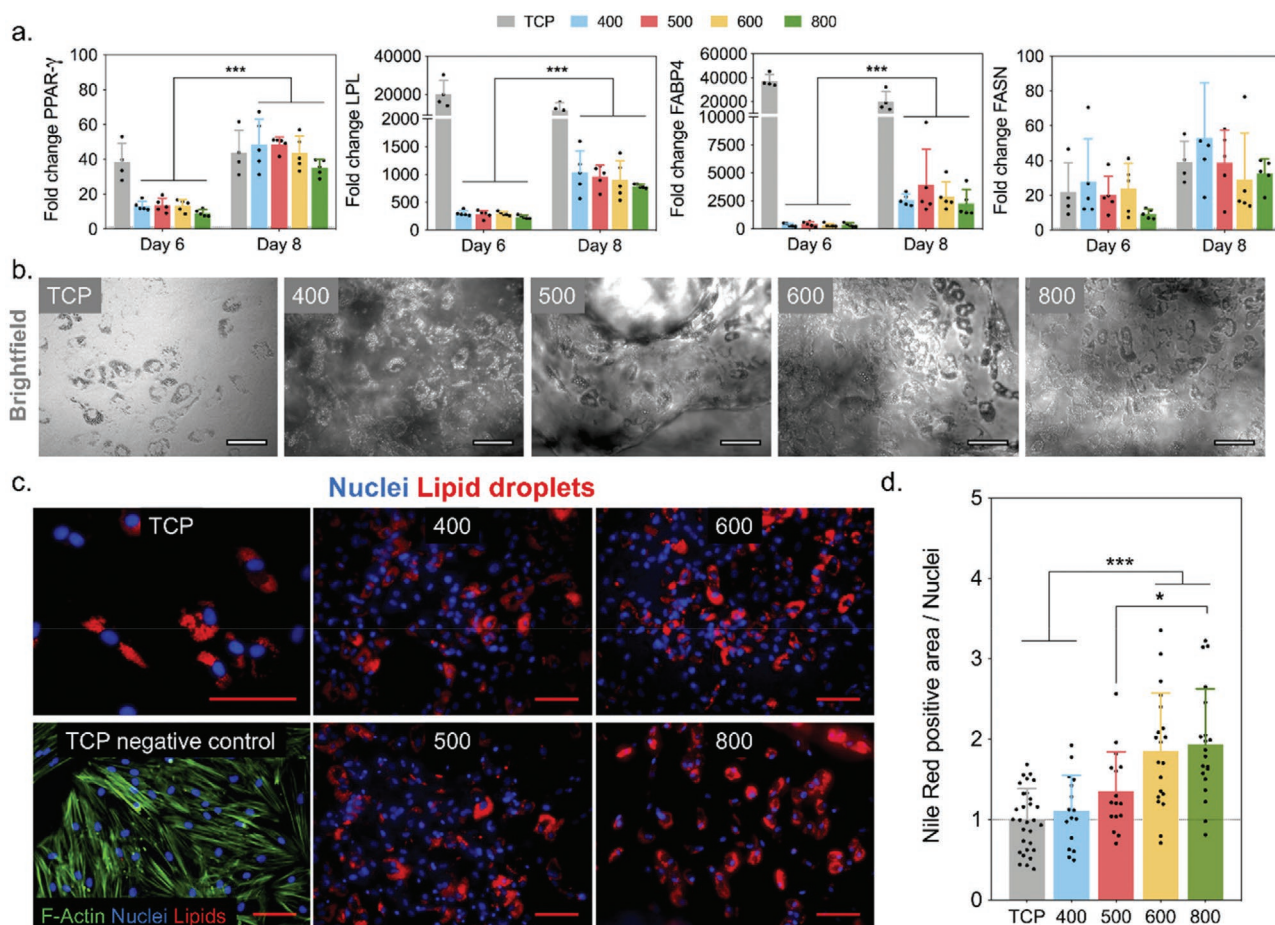


Figure 2. Adipogenic differentiation of MSCs on extrusion-printed scaffolds. a) Gene expression of the adipogenic markers PPAR- γ , LPL, FABP, and FASN by MSCs on TCP compared to the scaffolds. b) Brightfield and c) immunofluorescent images showing clearly visible lipid droplets after 8 days of culture in adipogenic media. d) Quantification of adipogenic differentiation by normalizing Nile Red (stains lipid droplets) area to the number of nuclei. The scale bars represent 200 μm in all images except TCP panel in (c) where it is 100 μm .

to their biological history and relevance have been used frequently for adipose tissue engineering, MSCs from the bone marrow can be similarly potent at differentiating into the adipogenic lineage.^[19] Because gene expression results did not show evidence that adipogenic differentiation occurred preferentially in any one of the pore size scaffolds, we wondered if there were differences in the spatial distribution of differentiated cells within the scaffolds. Therefore, cellular infiltration and spatial distribution of differentiated MSCs was investigated in a subsequent step.

For scaffolds of all tested pore sizes, pronounced staining signals for both cell nuclei and lipid droplets are visible in the top region (Figure 3a). This finding goes in line with MSCs having been seeded from the top onto the scaffolds during the cell culture experiment. While there is little to no difference observable between the scaffolds with strut spacings of 400 μm and 500 μm , with further increasing pore size, more staining signals are observable in the mid and bottom regions. Adipogenically differentiated MSCs co-located with cell nuclei can be observed throughout the scaffold and for all pore sizes.

Figure 3b shows the relative cell distribution for scaffolds of each pore size. For scaffolds with strut spacings of 400 and 500 μm , more than 75% of all cells were found in the top region, less than 20% in the mid region, and less than 10% in the bottom region. In comparison, scaffolds with spacing

of 600 μm had significantly less cells ($\approx 60\%$) in the top region and correspondingly more cells in the mid ($\approx 30\%$) and bottom ($\approx 15\%$) regions. The largest pore size scaffolds had the most evenly distributed cells. More cells ($\approx 50\%$) were found in the mid region than the top region ($\approx 35\%$). Figure 3c depicts the relative distribution of areas of adipogenic differentiation (pixel intensity of lipid droplet positive areas) within the scaffolds, which followed very similar distribution trends to the one observed for cell nuclei, highlighting greater infiltration of cells and homogenous distribution of lipid droplets in the 3D constructs. One potentially straightforward way to improve cell distribution in large scale constructs with small pores could be to use bioreactor systems with continuous fluid flow or altering the viscosity of seeding solutions.^[20]

3D printed scaffolds can be useful platforms to grow adipose tissue in vitro or in vivo because they provide volumetric space that can be designed in accordance with patient needs. We found that MSCs differentiated robustly into the adipogenic lineage equally well in scaffolds of all pore sizes (200–600 μm). However, spatial distribution and cellular infiltration varied such that scaffolds with bigger pore sizes ($>500 \mu\text{m}$) support simultaneous differentiation and infiltration. These findings show the crucial importance of considering design parameters such as pore size when designing scaffolds for 3D soft tissue regeneration.

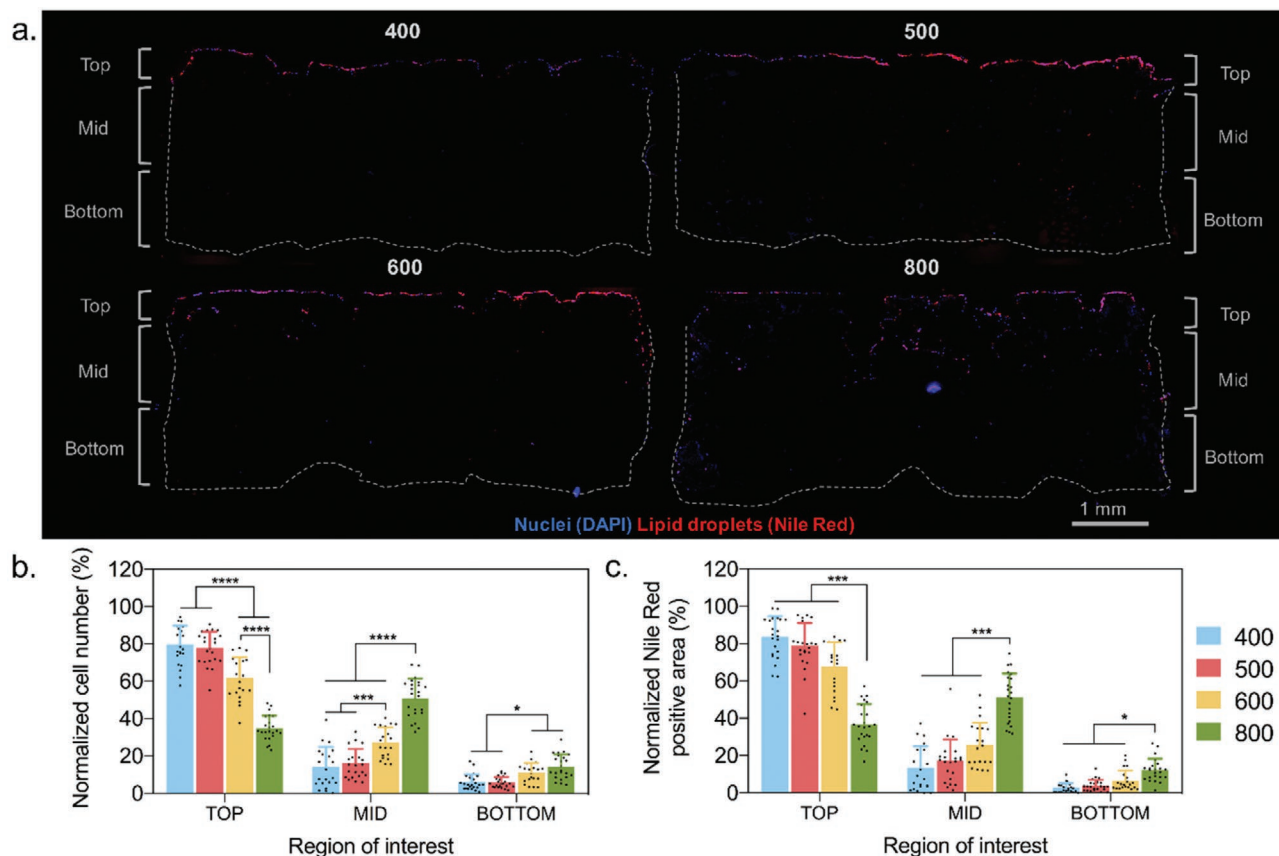


Figure 3. Spatial distribution of cells and lipid droplets in scaffolds. a) Representative scaffold cross sections stained with DAPI (nuclei) and Nile Red (lipid droplets) on each scaffold type showing differences in cell infiltration and spatial distribution of adipogenically differentiated cells. Quantification of b) cell and c) Nile Red positive area in different regions of the scaffold.

Experimental Section

Material Development and Scaffold Fabrication via Extrusion-Based 3D Printing: Gelatin type B (Rousselot, Ghent, Belgium) was modified with methacrylic anhydride (Sigma-Aldrich, Diegem, Belgium) to introduce methacrylamide functionalities according to the protocol of Van Den Bulcke et al.^[21] ¹H NMR spectroscopy (Bruker Avance II, 500 MHz) was applied to determine the degree of substitution (DS) of 97%.^[22] An aqueous solution consisting of 10 w/v Gel-MA and 2 mol% photo-initiator lithium (2,4,6-trimethylbenzoyl) phenylphosphinate (LAP) with respect to the photo-crosslinkable moieties was prepared for scaffold fabrication.^[23] Next, the printer cartridge containing the polymer solution was placed at 4 °C to induce physical gelation obtaining a viscous solution. The scaffolds were produced using the Bioscaffolder 3.1 from GeSIM (Radeberg, Germany). A CAD model consisting of a cuboidal design with a length of 5.9 mm and a height of 2.57 mm was created. The scaffolds were printed using a precision nozzle with a diameter of 150 μm. The temperature of the cooling plate, the printing temperature, the pressure, and the writing speed were optimized to 5 °C, 30 °C, 120 kPa, and 10 mm s⁻¹, respectively. UV-induced (365 nm) polymer crosslinking was realized by irradiating every printed layer for 10 s.

Physico-Chemical Characterization of the Printed Scaffolds: Optical microscopy was applied to determine the pore size of the scaffolds. Quantification of the pore size was done using Fiji ImageJ software. The mass swelling ratio of the scaffolds was determined by submerging the printed structures in double distilled water at 37 °C for 24 h. The scaffolds were then weighed (m_s) after excess water was removed. Subsequently, the scaffolds were lyophilized and weighed again to obtain the dry mass of the scaffold (m_d). The mass swelling ratio was calculated using following formula

$$\text{Mass swelling ratio} = \frac{m_s}{m_d}$$

The compressive modulus of the scaffolds was measured using a Tinius Olsen 5ST (Horsham, USA) equipped with the Horizon software. Equilibrium swollen scaffolds were applied for the compression tests using a 25 N load cell. The experimental dimensions (i.e., width, length, and height) of each scaffold were determined with a Vernier caliper. Subsequently, a stress–strain plot was recorded during compression using a preload of 0.1 N, a preload speed of 1 mm min⁻¹ and a constant speed of 5 mm min⁻¹. The compressive modulus was derived from the slope of the stress–strain curve.

Cell Culture, Seeding, and Evaluation of Adipogenic Differentiation: All scaffolds were immersed for 1 h in 70% ethanol and subsequently washed with PBS at least three times prior to cell culture. Primary human bone marrow MSCs were expanded under standard culture conditions (Dulbecco's low glucose Modified Eagle's Medium, 10% v/v fetal bovine serum, 1% v/v penicillin/streptomycin, 1% v/v Glutamax), and maintained in passages 3–5 for the experiments. MSCs were seeded on the scaffolds at a density of 2.5×10^5 cells per scaffold using custom-made silicone molds to maximize cell attachment. After overnight culture in the molds, the cell seeded scaffolds were transferred to new wells and the culture media were refreshed. For adipogenic differentiation experiments, cell seeded scaffolds were cultured in adipogenic medium (dexamethasone 1 μM, insulin 1 μM, 3-Isobutyl-1-methylxanthine 500 μM, indomethacin 100 μM, in high glucose media) for 6 and 8 days. At these time points, the scaffolds were either fixed for microscopy, cryoembedded for sectional analysis (see below) or assessed for gene expression. For gene expression analysis, the cell seeded scaffolds were first washed with PBS and RNA was isolated using the Qiagen RNeasy mini kit, according to the manufacturer's instructions. The RNA concentration was quantified using a nanodrop spectrophotometer. cDNA was synthesized using the iScript Reverse Transcription Supermix. SYBR Green dye was used to detect fluorescence. The amplification profile was assessed using a LightCycler 480 (Roche, Germany). Gene expression was quantified using the ddCt method and fold change was calculated using the

formula 2^{-ddCt} . Values for the genes of interest were normalized to the housekeeping gene (ACTB). The primers are listed in Table S1, Supporting Information. To enable the evaluation of adipogenic differentiation by immunofluorescent staining and microscopy, cell seeded scaffolds were first washed with PBS, fixed with 4% formaldehyde for 10 min, permeabilized using 0.1% w/v Triton-X, and incubated with 0.1% v/v Nile Red dye and 1 μg mL⁻¹ DAPI. After several washings, lipid droplets and nuclei were imaged using an inverted fluorescence microscope (Leica, Germany). Multiple regions of interest were identified and images were acquired at multiple z-stacks. An ImageJ-based macro was used to quantify cell numbers using the DAPI channel in maximum projection images. Additionally, Nile Red positive pixel area was obtained using image thresholding. The total intensity per region of interest was normalized to the cell numbers.

Cryoembedding, Sectioning, and Histological Processing of Fixed Scaffolds: For cryoembedding, fixed scaffolds were incubated in a 5% sucrose in PBS solution for 15 min and subsequently in 30% sucrose in PBS overnight. The incubated scaffolds were immersed in Tissue-Tek O.C.T. compound (Sakura) for 1 h. Finally, the scaffolds were transferred into fresh Tissue-Tek compound and frozen in liquid nitrogen-cooled isopentane (Carl Roth). The scaffolds were transferred to -80 °C and stored until used. Cryoembedded scaffolds were sectioned at a thickness of 15 μm and fixed onto glass slides (SuperFrost Ultra Plus, Menzel-Gläser). For the histological analysis of the cryosections, cells were analyzed by fluorescence microscopy to quantify the cell number and distribution as well as adipogenic differentiation. To this end, the sections were first washed in PBS, blocked in a solution of 3% BSA-PBS, and stained with DAPI (1 μg mL⁻¹) and Nile Red (1 μg mL⁻¹). The stained sections were preserved in Fluoromount (SouthernBiotech, Fluoromount-G). Microscopical analysis was conducted using an inverted fluorescence microscope (DMI6000B, Leica, Germany). Fluorescence images were acquired as tile-scans of the scaffold sections with z-stack projection covering a total z-range of 12–15 μm. Image analysis was carried out using ImageJ software using a custom-made macro. The cross-sectional area of each scaffold was divided into three regions along the z-axis (top: 0–10%; mid: 10–40%; bottom: 40–100%; 0 represents surface where cells were seeded). For each scaffold, the cell number and the pixels of lipid staining of the individual regions were divided by the scaffold's total number of cell nuclei and total pixels of lipid staining, respectively. For each configuration, 21–24 cryo-sections from different scaffolds were analyzed.

Statistical Analysis: All data are shown as mean ± standard deviation, unless otherwise noted. Statistical analysis was carried out on GraphPad Prism software. When data were normally distributed, comparison between multiple groups was made using one-way ANOVA with Tukey's post-hoc test. When normality could not be assumed, comparisons were made using Kruskal–Wallis test with Dunn's multiple comparison test. Levels of statistical significance were set at: * $p < 0.05$, ** $p < 0.01$, *** $p < 0.001$, and **** $p < 0.0001$.

Supporting Information

Supporting Information is available from the Wiley Online Library or from the author.

Acknowledgements

L.T. and M.R.K. contributed equally to this work. S.V.V. and T.H.Q. contributed equally to this work as corresponding authors. L.T. would like to thank the Research Foundation Flanders (FWO) for providing her with an FWO-SB fellowship. Furthermore, S.V.V. would like to acknowledge the FWO for financial support via research grants (G005616N, G0F0516N, FWOKN273, G044516N, G056219, 1S26616N). T.H.Q. acknowledges funding from the German Research Foundation (DFG; Grant #QA-58/1-1).

Conflict of Interest

The authors declare no conflict of interest.

Keywords

adipogenic differentiation, extrusion-based 3D-printing, hydrogel, mesenchymal stromal cells, pore size

Received: October 11, 2019

Revised: December 19, 2019

Published online: February 20, 2020

-
- [1] F. Bray, J. Ferlay, I. Soerjomataram, R. L. Siegel, L. A. Torre, A. Jemal, *Ca-Cancer J. Clin.* **2018**, *68*, 394.
- [2] M. Doornaert, J. Colle, E. De Maere, H. Declercq, P. Blondeel, *Ann. Med. Surg.* **2019**, *37*, 47.
- [3] K. Waked, J. Colle, M. Doornaert, V. Cocquyt, P. Blondeel, *The Breast* **2017**, *31*, 128.
- [4] I. Van Nieuwenhove, L. Tytgat, M. Ryx, P. Blondeel, F. Stillaert, H. Thienpont, H. Ottevaere, P. Dubruel, S. Van Vlierberghe, *Acta Biomater.* **2017**, *63*, 37.
- [5] E. C. M. Mariman, P. Wang, *Cell. Mol. Life Sci.* **2010**, *67*, 1277.
- [6] J. Van Hoorick, P. Gruber, M. Markovic, M. Rollot, G. Graulus, M. Vagenende, M. Tromayer, J. Van Erps, H. Thienpont, J. C. Martins, S. Baudis, A. Ovsianikov, P. Dubruel, S. Van Vlierberghe, *Macromol. Rapid Commun.* **2018**, *39*, 1800181.
- [7] S. Van Van Vlierberghe, P. Dubruel, E. Schacht, *Biomacromolecules* **2011**, *12*, 1387.
- [8] B. Huber, K. Borchers, G. E. M. Tovar, P. J. Kluger, *J. Biomater. Appl.* **2016**, *30*, 699.
- [9] L. Kessler, S. Gehrke, M. Winnefeld, B. Huber, E. Hoch, T. Walter, R. Wyrwa, M. Schnabelrauch, M. Schmidt, M. Kückelhaus, M. Lehnhardt, T. Hirsch, F. Jacobsen, *J. Tissue Eng.* **2017**, *8*, 204173141774415.
- [10] S. M. Peltola, F. P. W. Melchels, D. W. Grijpma, M. Kellomäki, *Ann. Med.* **2008**, *40*, 268.
- [11] E. Y. S. Tan, W. Y. Yeong, *Int. J. Bioprinting* **2015**, *1*, 49.
- [12] W. Liu, M. A. Heinrich, Y. Zhou, A. Akpek, N. Hu, X. Liu, X. Guan, Z. Zhong, X. Jin, A. Khademhosseini, Y. S. Zhang, *Adv. Healthcare Mater.* **2017**, *6*, 1601451.
- [13] D.-M. Liu, *Ceram. Int.* **1997**, *23*, 135.
- [14] Z. Li, H. R. Ramay, K. D. Hauch, D. Xiao, M. Zhang, *Biomaterials* **2005**, *26*, 3919.
- [15] T. H. Qazi, L. Tytgat, P. Dubruel, G. N. Duda, S. Van Vlierberghe, S. Geissler, *ACS Biomater. Sci. Eng.* **2019**, *5*, 5348.
- [16] A. J. Engler, S. Sen, H. L. Sweeney, D. E. Discher, *Cell* **2006**, *126*, 677.
- [17] S. Ansari, C. Chen, M. M. Hasani-Sadrabadi, B. Yu, H. H. Zadeh, B. M. Wu, A. Moshaverinia, *Acta Biomater.* **2017**, *60*, 181.
- [18] C. Brännmark, A. Paul, D. Ribeiro, B. Magnusson, G. Brolén, A. Enejder, A. Forslöv, *PLoS One* **2014**, *9*, e113620.
- [19] S. P. Hoo, Q. L. Loh, Z. Yue, J. Fu, T. T. Y. Tan, C. Choong, P. P. Y. Chan, *J. Mater. Chem. B* **2013**, *1*, 3107.
- [20] M. Cámara-Torres, R. Sinha, C. Mota, L. Moroni, *Acta Biomater.* **2019**, *101*, 183.
- [21] A. I. Van Den Bulcke, B. Bogdanov, N. De Rooze, E. H. Schacht, M. Cornelissen, H. Berghmans, *Biomacromolecules* **2000**, *1*, 31.
- [22] L. Tytgat, M. Markovic, T. H. Qazi, M. Vagenende, F. Bray, J. C. Martins, C. Rolando, H. Thienpont, H. Ottevaere, A. Ovsianikov, P. Dubruel, S. Van Vlierberghe, *J. Mater. Chem. B* **2019**, *7*, 3100.
- [23] M. Markovic, J. Van Hoorick, K. Hölzl, M. Tromayer, P. Gruber, S. Nürnberger, P. Dubruel, S. Van Vlierberghe, R. Liska, A. Ovsianikov, *J. Nanotechnol. Eng. Med.* **2015**, *6*, 021001.